Electronic Supplementary Material (ESI) for Chemical Communications

Versatile chemical tool for the preparation of conductive graphene-based polymer nanocomposites.

Marta Castelaín, Gerardo Martínez, Gary Ellis, Horacio J. Salavagione

Full Experimental Details.

Materials.

Graphene (Angstron Materials), Polyethylene monoalcohol (PE-OH, M.W = 460 g.mol^{-1}, Aldrich), carbon tetrabromide (Aldrich), sodium hydrogenosulfide (NaSH, Aldrich), 2,2'-azobis(2-methylpropionitrile) (AIBN, Aldrich) α,α-dimethoxy-α-phenylacetophenone(Aldrich), toluene (Merck) and o-dichlorobenzene (Aldrich) were used as received without further purification.

A commercial high density polyethylene (HDPE, M.F.I = 0.15 dl.10min^{-1} (2.16 kg), density = 945kg.m^{-3}) was kindly supplied by Repsol, Spain.

Solvents and reagents were dried by the usual methods prior to use and typically used under inert gas atmosphere.

Graphene for surface modification was monolayer grown on Si/SiO_2 substrate (Graphenea, Spain).

Characterization.

NMR spectra were recorded on a Varian Inova 400 MHz spectrometer and chemical shifts (δ) are reported in ppm and referenced to the residual solvent signal. The splitting patterns are designated as follows: s=singlet, d=doublet, t=triplet, m=multiplet.

Infrared spectra were recorded on a Perkin–Elmer System 2000 FTIR spectrometer. The samples were mixed with KBr and compressed pellets were prepared for analysis in the spectral range ν=4000–500 cm^{-1} at a resolution of 4 cm^{-1}. All spectra were baseline corrected.

Raman measurements were made in the Raman Microspectroscopy Laboratory of the Characterization Service in the Institute of Polymer Science & Technology, CSIC. A Renishaw InVia Reflex Raman system (Renishaw plc.,Wotton-under-Edge, UK) was used employing a grating spectrometer with a Peltier-cooled charge-coupled device (CCD) detector, coupled to a confocal microscope. All spectra were processed using Renishaw WiRE 3.2 software. The Raman scattering was excited using an Argon ion laser wavelength of 514.5 nm. The laser beam was focused on the sample with a 100 microscope objective (N.A. = 0.85), with a laser power at the sample of approximately 2mW.

Thermogravimetric analysis were carried out using a TA Instruments Q50 thermobalance at a heating rate of 10 °C min^{-1}, from 50 to 800 °C under an inert atmosphere (nitrogen, 60 cm^3 min^{-1}). Samples were analysed using TA Instruments Universal Analysis 2000 software (version 4.5A, Build 4.5.0.5).

The crystallization and melting behavior were investigated by DSC using a Mettler TA4000/DSC30. The experiments were carried out under nitrogen using ~5 mg samples sealed in aluminum pans. The samples were heated from 0 to 140 ºC, maintained at this temperature for 5 min, then cooled to 0ºC and heated again to 140 ºC. Heating and cooling rates of 10 ºC min^{-1} were used in all cases. The transition temperatures were taken as the peak maxima in the calorimetric curves.

The X-ray diffractograms (XRD) of the samples were obtained using a Bruker D8-Advanced X-ray generator (CuKα) operated at 40 kV and 40 mA. For alkyne modified graphene and mG-SPE the diffractograms were

collected from powder samples, whilst for graphene and G-SPE the samples employed were pressed-pellets because of static electricity in the powders.

DC-conductivity measurements were carried out using the four-probe method on pellets or films perfectly dried under vacuum 24h. In the case of G-SPE/PE-OH nanocomposites, which have high amounts of graphene, pellets of 13 mm diameter were prepared. In the case of nanocomposites of high molecular weight polyethylene (HDPE) and PE-OH/G-SPE50 (low graphene content) as filler, hot-pressed films were prepared and cut into rectangles (about 0.6 cm wide and 1.2 cm long). The measurements were carried out using a four-probe setup equipped with a dc low-current source (LCS-02) and a digital micro-voltmeter (DMV-001) from Scientific Equipment & Services. The conductivity was calculated by using the following equation:

$$\sigma = 1/\rho = 4.5324\left(\frac{V}{I}\right) f_1 f_2$$

where *t* is the thickness of the sample, f_1 is the finite thickness correction for thick samples on an insulating bottom boundary and f_2 is the finite width correction. The thickness correction is described by the following equation:

$$f_1 = \frac{\ln(2)}{\ln\left[\frac{\sinh(t/s)}{\sinh(t/2s)}\right]}$$

where *s* is the probe distance (0.2 cm). The width correction f_2 is a function of the shape of the sample thickness and length (*l*) for rectangular samples and thickness and diameter for circular samples.

Synthetic procedure for the preparation of PE-SH

In the first step polyethylene monoalcohol was converted to the bromide derivative (PE-Br). A solution containing PE-OH (3.0 g, 6.5 mmol) and carbon tetrabromide (2.9 g, 8.7 mmol) in toluene (120 mL) was added to a 500 mL flask and then heated at 65 ºC under magnetic stirring until completely dissolved. After cooling to room temperature, a solution of triphenyl phosphine (2.5 g, 9.5 mmol) in 10 mL of toluene was added dropwise. The mixture was stirred 20 minutes more at room temperature, and then reheated to 65 ºC for 3 more hours. The white precipitate formed was filtered, and the remaining solution was precipitated with acetone, obtaining 1.5 g of PE-Br product (yield = 67%).
^{1}H-NMR (400 MHz, [D_8] toluene, 80 ºC), δ (ppm): 0.91 (t, 3H, -CH_3), 1.35 (Br, 2nH, CH_{2n}), 1.58 (m, CH_2-CH_2-Br), 3.01 (t, 2H, CH_2-Br).

Subsequently the bromines were converted to thiols using a variant of a previously reported procedure.[1] Briefly, a solution containing PE-Br (2.66 g, 5.09 mmol) in toluene (80 mL) was heated to 100 °C, and a solution of NaSH (2.80 g, 0.05 mol) in DMF (10 mL) was added. After a 90 min reaction time the resulting mixture was cooled down slowly to room temperature and filtered. Then the product was washed with methanol and water and dried under vacuum.
^{1}H-NMR (400 MHz, [D_8] toluene, 80 ºC), δ (ppm): 0.91 (t, 3H, -CH_3), 1.07 (t, 1H, -SH), 1.35 (Br, 2nH, CH_{2n}), 1.66 (q, 4H, CH_2-CH_2-SH), 2.23 (c, 2H, CH_2-SH), 2.60 (t, 2H, CH_2-SH), yield = 80%.

Scheme S1. Synthetic protocol to prepare PE-SH used in thiol-radical click reactions

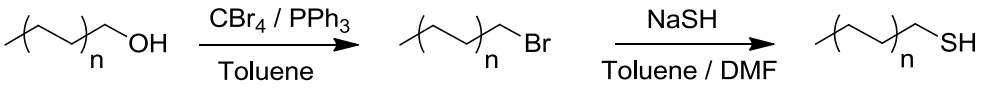

PE-SH displays slightly improved thermal properties than the starting PE-OH. The TGA curves show that the onset of thermal degradation shifts to higher temperature by ~100 ºC although the temperature of maximum degradation rate are similar for both samples. The better stability of PE-SH is due to the elimination of less-stable fragments of the PE-OH through the synthetic procedure carried out to prepare PE-SH (scheme S1). This is clearly seen by DSC, where the heating scan of the starting PE-OH shows broader melting signals than the PE-SH. The sharper process in the case of PE-SH is because the chain distribution of this sample is more homogeneous than that of the starting PE-OH.

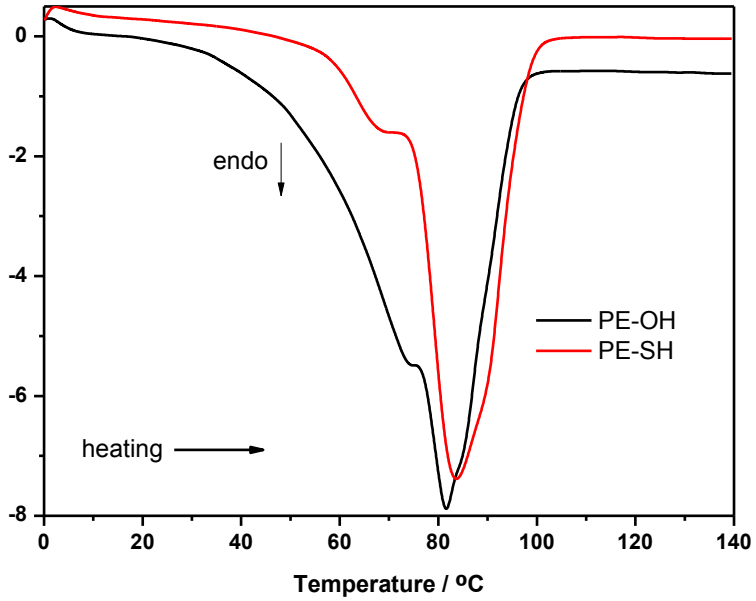

Figure S1. DSC heating scan of PE-OH and PE-SH. Scan rate = 10ºC.min^{-1}

The PE-SH was then used in the thermally initiated thiol-radical modification of graphene. Both thiol-ene and thiol-yne click reactions were addressed. In the former the reaction was conducted on pristine graphene, while in the latter the graphene was previously functionalized with alkyne moieties. Alkyne-modified graphene was prepared following synthetic procedures reported elsewhere.[2]

Thiol-ene click reaction. The thermal-initiator, (AIBN 1.72 g, 0.01 mol) and graphene (0.5 g) were added onto a solution of PE-SH (0.5 g) in 50 mL of anhydrous o-DCB, under nitrogen atmosphere. The mixture was heated at 70 °C overnight. The solid product was collected by filtration and washed with methanol and hot toluene to remove the rest of initiator and non-reacted polymer, respectively. The product was denominated G-SPE.

Thiol-yne click reaction. AIBN (1.72 g, 0.01 mol), and alkyne modified graphene (0.25 g) were added to a solution of PE-SH (0.5 g) in 50 mL of anhydrous o-DCB under nitrogen atmosphere. The mixture was heated at 70 °C overnight. The solid product was collected by filtration and washed with methanol and hot toluene

to remove the rest of initiator and non-reacted polymer, respectively. The product was denominated mG-SPE.
^{1}HNMR (400 MHz, [D_8] toluene, 80 ºC), δ (ppm): 0.91 (t, 3H, -CH_3), 0.96 (m), 1.35 (br, 2nH, CH_{2n}), 1.66 (q, 4H, CH_2-CH_2-S), 2.42 (t, 1H, S-C*H*-CH_2-S), 2.60 (t, 2H, CH_2-S).

Characterization.
Figure S2 shows the infrared spectra of PE-SH, G-SPE and mG-SPE. All the polyethylene bands can be clearly observed in the case of mG-SPE at 2919/2849 cm^{-1} (CH_2 symmetric and anti-symmetric stretching), 1472/1463 cm^{-1} (CH_2 bending) and 730/718 cm^{-1} (CH_2 rocking), but only the most intense appear in G-SPE. The spectrum of mG-SPE also shows evidence of bands originating from the aromatic groups of the starting alkyne-modified graphene at 1668, 1595, 1503, 1174 and 837 cm^{-1}.

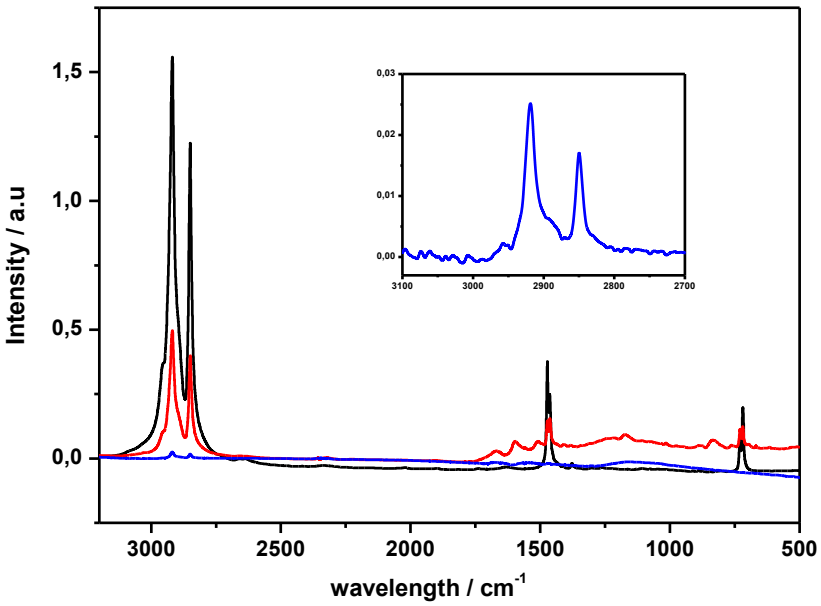

Figure S2 FTIR transmission spectra of PE-SH (black), mG-SPE (red) and G-SPE (blue). The inset shows a magnification of the methylene stretching region for G-SPE

Raman spectroscopy also demonstrates the success of the reaction, but in a more indirect manner (Figure S3). The original signals of the PE-SH (black curve) are completely masked by the signals of graphene, due to the high Raman efficiency of the D and G bands. In addition, in the case of mG-SPE (red curve) the graphene bands are seen on top of a broad fluorescence band originating from the pendant aromatic groups.

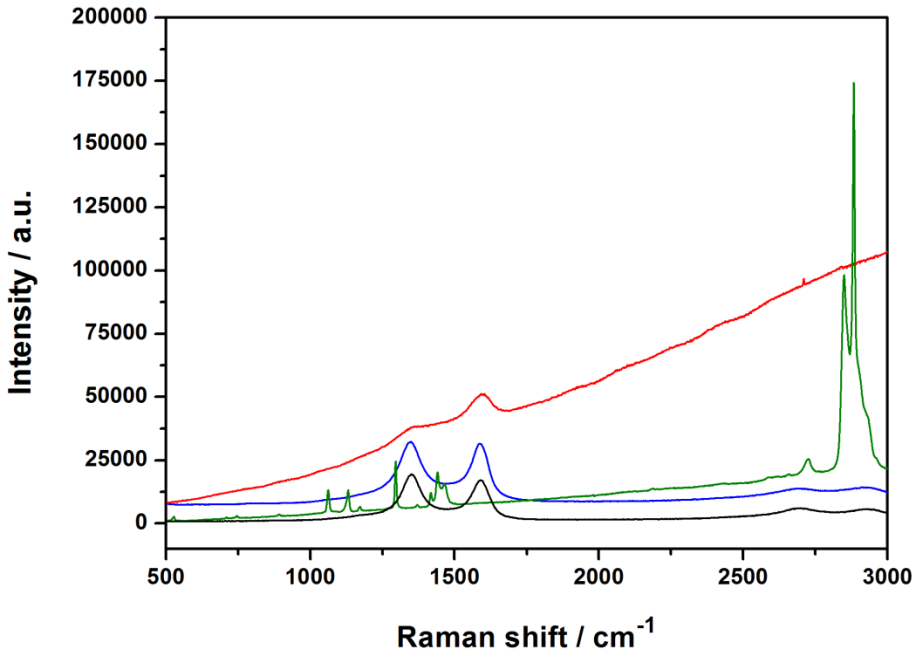

Figure S3. Raman spectra of starting graphene (black line), PE-SH (green), G-SPE (blue) and mG-SPE (red).

In the ^{1}H NMR spectrum of mG-SPE (Figure S4) it can be clearly perceived that the SH signal of PE-SH completely disappears after the thiol-yne click reaction. In addition, new signals appeared in the clicked product, including a multiplet at δ= 6.63-6.61 originated in the aromatic protons of the starting modified graphene and a triplet at 2.42 ppm that can be assigned to the proton noted as A in Figure S4. In the case of G-SPE the low solubility prevented reaching minimum values of concentration in order to obtain a reasonable spectrum.

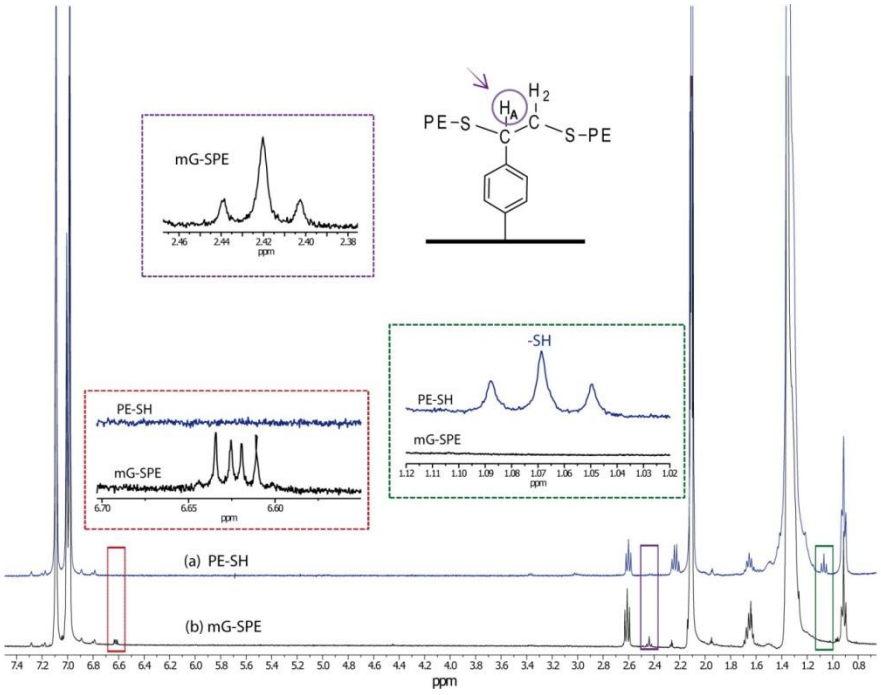

Figure S4. ^{1}HNMR spectra of PE-SH and mG-SPE. The insets show enlarged views of the thiol and aromatic protons, where the disappearance of the thiol proton as well as new aromatic proton signals can be noted.

The XRD diffractograms of all samples are shown in Figure S5. Note that not all curves correspond to the same intensity scale because the samples were collected in powder and in pressed pellets. However, there are several points to highlight. It is clear that after the functionalization with alkyne groups, the graphite-like peak of graphene shifted to lower angles, from 25.7-26º to 18.4-20º. This is due to the increase in the interlaminar distance (I_d) between graphene sheets to 0.48 nm (I_d of graphite-like structures is 0.34 nm). Comparing with the thiol-clicked products, slight differences can be seen in the case of graphene and G-SPE due to the low degree of functionalization (I_d = 0.36 nm). However, in the case of mG-SPE the pattern is markedly different as two narrow crystalline peaks on the top of the background from amorphous material are clearly distinguished. Both peaks correspond to crystalline planes of the polymer as shown in the orange curve in Figure S5.

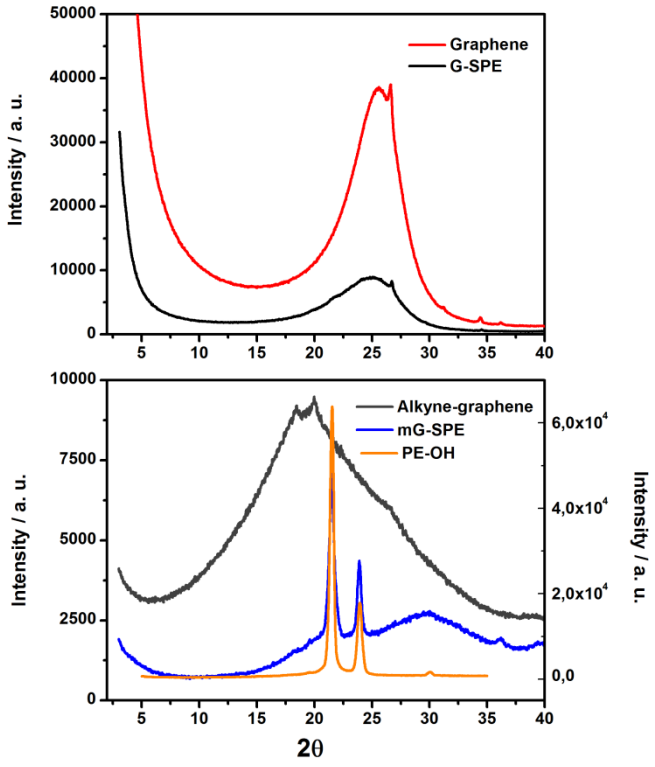

Figure S5. Top: XRD patterns obtained from pressed pellets of graphene (red curve) and G-SPE (black). Bottom: XRD patterns obtained from powder samples of alkyne-modified graphene (grey), mG-SPE (blue) and starting PE-OH (orange, the intensity of this sample correspond to the right-hand *y*-axis).

The amount of polymer was determined by TGA. For chemically-modified graphene it is widely accepted that the residue after heating up to 800 º C can be used to determine the graphene content, and therefore the degree of modification.[3,4,5,6,7,8] It is clear that this technique does not discriminate between covalent and adsorbed species and a study has been conducted in our laboratory clarify this.[9] In this case the TGA curve for mG-SPE displays only one process corresponding to the degradation of the covalently attached polymer. In the case of G-SPE it seems that the total weight loss occurs in two processes. The process

observed at lower temperature can, in principle be associated to non-covalently bonded PE-SH chains that may be aligned with those chain covalently bonded. Meanwhile the latter weight loss can be assigned to the elimination of covalently linked PE chains. To prove this the G-SPE sample was further processed by Soxhlet extraction in hot toluene by 12 h in order to wash out the physically connected polymer chains. The solid in the Soxhlet cartridge was then analyzed by TGA to check the disminution on the first process but the curve was similar to that shown in Figure 1. In fact the contribution of the first process to the total weight loss was slightly higher in the case of the Soxhlet extracted sample.

Preparation of composites of G-SPE and PE-OH.

In order to analyze the effect of the polymer modification of graphene in the interfase of graphene-based polyethylene nanocomposites, we first prepared high graphene-content composites of G-SPE and PE-OH. Different amounts of SPE and PE-OH to obtain a final mass of 400 mg were dispersed together in 20 mL of warm xylene (90ºC) under vigorous stirring. Subsequently the mixtures were precipitated in huge amounts of methanol, filtered, washed with methanol and thoroughly dried under vacuum. Thus, composites containing 10, 20 and 50 wt. % of G-SPE were prepared and denominated PE/G-SPE*x*, where *x* denotes the percentage of G-SPE. The thermal properties of the materials were studied by DSC and TGA, whilst the electrical conductivity was measured by the four-probe method.

DSC results show that all nanocomposites have a narrower melting range than the pure polymer because of further purification arising from the dissolution/precipitation/washing preparation procedure (Figure S6) that results in the loss of lower molecular mass fragments. In addition the melting peak slightly shifts with the G-SPE content (inset). The main difference with respect to the PE-OH occurs at lower G-SPE contents, while at higher filler loadings the thermograms resemble that of the polymer. This is due to the fact that the G-SPE concentration is too high and the sheets tend to agglomerate.

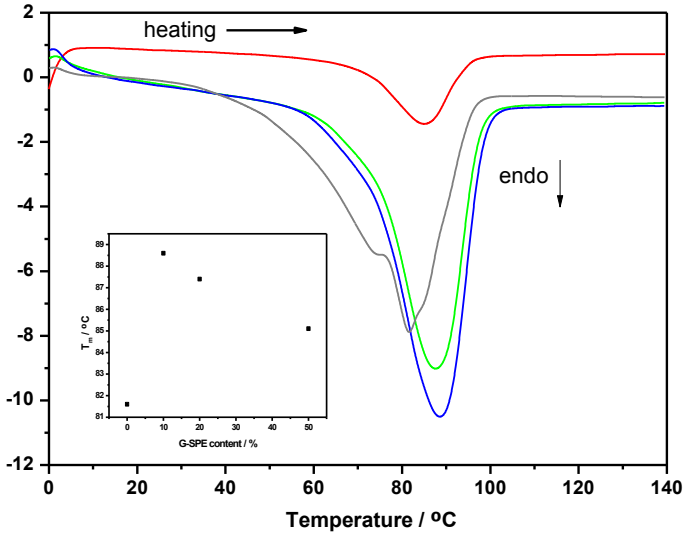

Figure S6. DSC heating scan of PE-OH (grey line) and its composites PE/G-SPE10 (blue), PE/G-SPE20 (green) and PE/G-SPE50 (red). Scan rate = 10ºC.min^{-1}. The inset shows the variation of the melting temperature with the G-SPE content.

The thermal stability of all nanocomposites is better than that of the pure polymer in terms of onset of degradation and temperature at maximum degradation rate (Figure S7). Among the nanocomposites, PE/G-SPE50 displays a somewhat lower onset of degradation, probably due to the excess of graphene (having higher thermal conductivity) that catalyzes the polymer decomposition. From the residual weight of the TGA curves it can be seen that the content of graphene in the PE/G-SPE50 sample is lower than that in the feed, being approximately 41 % instead of 50%. This value is important to determine the actual content of graphene in HDPE nanocomposites using PE/G-SPE50 as filler.

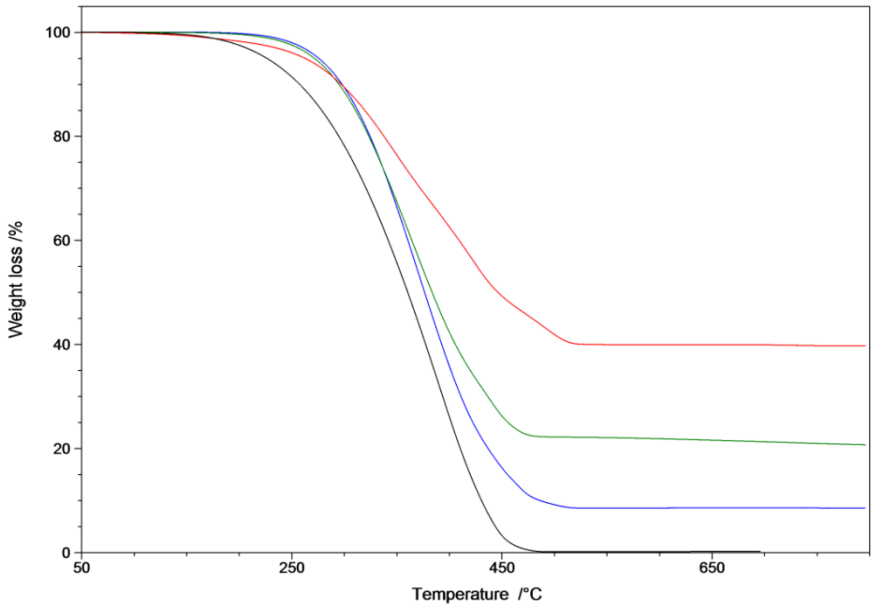

Figure S7. TGA curves of PE-OH (black), PE/G-SPE10 (blue), PE/G-SPE20 (green) and PE/G-SPE50 (red). Conditions: N_2, 10ºC.min^{-1}.

The conductivity of PE/G-SPE*x* composites was measured by using the four-probe method on pressed-pellets because the materials were not able to form films by melting due to the low molecular weight polymer used. The conductivity of the composites decreases as the G-SPE content decreases, which is reasonable because of the presence of graphene in the G-SPE.

Table S1. Conductivity values for the composites and nanocomposites prepared in this study

Sample	Sample type	Polymer	Filler content (wt. %)	Graphene content (wt. %)	DC value (S.cm^{-1})
ALK-graphene	Pellet				6E^{-4}
mG-SPE	Pellet				1.5E^{-4}
G-SPE	Pellet				12.6
PE/G-SPE10	Pellet	PE-OH	G-SPE_ 10	8.2	0.05
PE/G-SPE20	Pellet	PE-OH	G-SPE_ 20	16.4	0.6
PE/G-SPE50	Pellet	PE-OH	G-SPE_ 50	41	1
HDPE	Film	HDPE	0		1E^{-14}
HDPE/G1	Film	HDPE	PE/G-SPE50_ 1	0.41	1E^{-14}
HDPE/G2	Film	HDPE	PE/G-SPE50_ 2	0.82	1E^{-7}
HDPE/G3	Film	HDPE	PE/G-SPE50_ 3	1.23	8.4E^{-4}
HDPE/G5	Film	HDPE	PE/G-SPE50_ 5	2.05	0.02
HDPE/G10	Film	HDPE	PE/G-SPE50_ 10	4.1	0.270

Preparation of nanocomposites of PE/G-SPE50 and HDPE

Considering the results shown in Figures S6 and S7 as well as in Table S1 we chose the sample PE/G-SPE50 as a filler for mixing with high molecular weight polyethylene (HDPE, F.I = 0.11 g.10min^{-1}). Nanocomposites of HDPE and PE/G-SPE50 at different ratios were prepared as follows: different amounts of PE/G-SPE50 and HDPE to obtain a final mass of 200 mg were dispersed in 20 mL warm xylene (90ºC). The nanocomposites were collected by coagulation in methanol, and then filtered, washed with methanol and fully dried under vacuum. The nanocomposites were denominated HDPE/G*x*, where *x* denotes the final content of the filler PE/G-SPE50.

The modified graphene disperses reasonably well in the polymeric matrix indicating good interfacial interactions (Figure S8). Fig. S8 shows the SEM images of the fracture surface of samples containing 1 wt. % of the PE/G-SPE50 filler, where a nanocomposite of HDPE with non-functionalized graphene (HDPE-GC) prepared under identical conditions (Fig. S8 B) and the pure HDPE (Fig. S8 A) are also shown for comparison. This reference sample is somewhat heterogeneous having regions composed of pure polymer along with regions where the graphene seems better dispersed. However, for the PE/G-SPE50 sample it can be seen that the graphene laminates are perfectly dispersed in the polymer matrix throughout the sampled area

Although the scope of this technique does not allow the analysis of samples at a molecular scale to check the formation of the gradient interphase, the results suggest that the employed methodology (consisting in short-chain PE-functionalization of graphene, mixing with short-chain PE and mixing with HDPE) is useful to improve the graphene dispersion and therefore the graphene/polymer interfase.

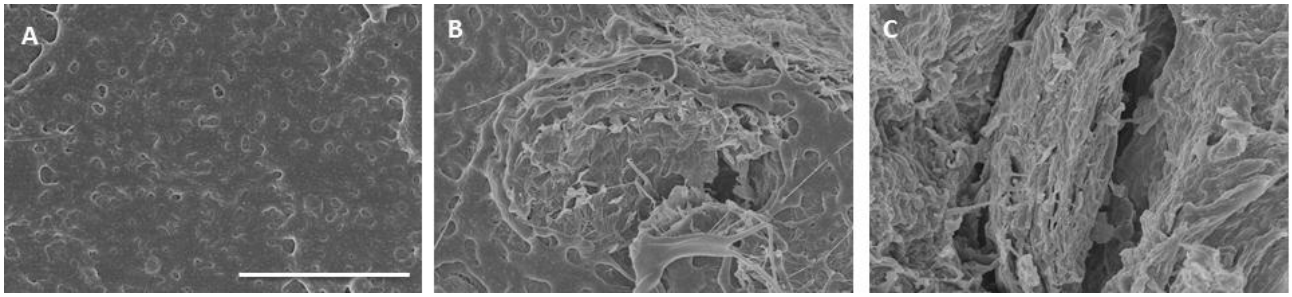

Figure S8. SEM images of HDPE (A), HDPE-GC (B) and HDPE/G1 (C). Scale bar in A applies to all images and correspond to 5 μm.

This improved interface observed by SEM translates in changes in the crystallization behavior of the polymer (Figure S9). The Figure S9 shows that the crystallization peaks did not change for the nanocomposites with 1 wt. % of the filler (0.41 wt. % of graphene) while for the samples with the higher amount of filler, T_{cryst} shifts to lower temperatures suggesting higher difficulty to form crystals. In addition the shape of the thermograms dramatically changes for the sample containing 10 % filler (4.1 wt. % of graphene). Moreover, the degree of crystallinity is also significantly altered by the presence of graphene. For the sample with 1 wt. % filler (0.41 wt. % of graphene) the crystallinity decreases by around 3 % (Table S2). However, the effect is more pronounced as the amount of filler increases, reaching over 60 % for the sample with 10 % filler (4.1 wt. % of graphene). These changes are clear evidence of the effective dispersion of the graphene into the HDPE matrix and the strong interface obtained by the gradient methodology. This can be explained by the existence of hydrophobic van de Waals interactions between the polymer brushes on graphene and the HDPE chains, to the detriment of hydrophobic interactions amongst the polymer chains that diminishes the crystallinity.

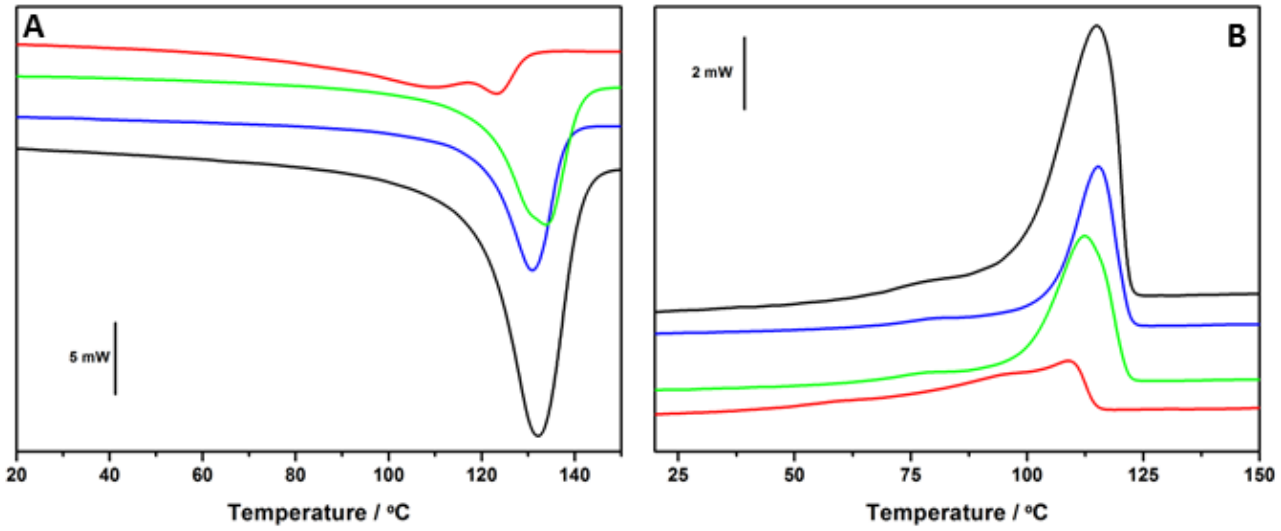

Figure S9. DSC heating (A) and cooling (B) curves of hot-pressed films of HDPE and the composites HDPE/G1 (blue), HDPE/G2 (green) and HDPE/G10 (red). Scan rate = 10ºC.min^{-1}

Table S2. List of the parameters obtained from the crystallization curves of HDPE and HDPE/Gx nanocomposites.

Sample	T_{cryst} (ºC)	ΔH_{cryst} (J.g^{-1})	Crystallinity loss (%)
HDPE	115	175.5	
HDPE/G1	115	170.3	2.9
HDPE/G2	112	171.6	2.2
HDPE/G10	109*	69.8	60.2

*Obtained from the first crystallization peak in the cooling scan.

Finally, the TGA curves show that the thermal stability, one of the good properties of this polymer, remains almost unaltered by the presence of the filler (Figure S10). Only the sample with the highest amounts of PE/G-SPE is slightly less stable.

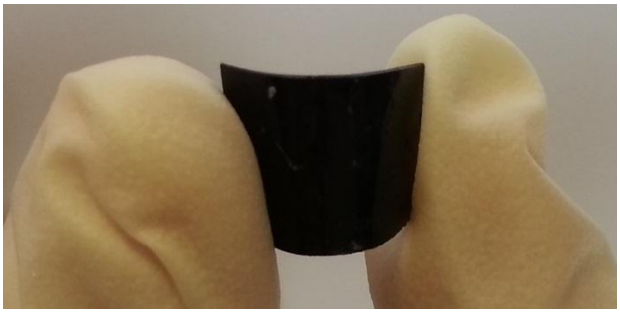

Figure S10. Photo showing the flexibility of one of the films used for electrical conductivity test.

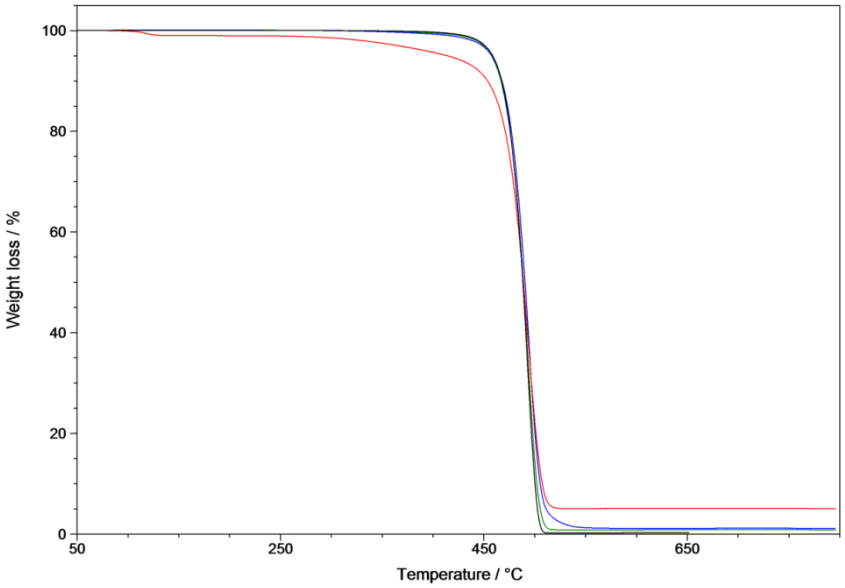

Figure S11. TGA curves of PE-OH (black), PE/G-SPE10 (blue), PE/G-SPE20 (green) and PE/G-SPE50 (red). Conditions: N_2 , 10ºC.min^{-1}.

The electrical conductivity of HDPE/G*x* was measured by the four-probe method on films prepared by melting the nanocomposites at 140ºC for 10 minutes. It is worth noting that the absolute values cannot be directly compared with those obtained for PE/G-SPEx because of differences in the sample preparation. In this case the melting process may lead to a better dispersion of the filler into the polymeric matrix.

Table S1 shows the variation of the electrical conductivity of the nanocomposites with filler content.

Photo-initiated thiol-ene modification of graphene

A 1cm^2 Si/SiO_2 wafer covered with high quality monolayer graphene was used as starting material. The surface was covered by few drops of a mixture containing the polymer (PE-SH, 50 mg) and the initiator α,α-dimethoxy-α-phenylacetophenone (0.6 mg) in 100 mL of warm toluene. After elimination of the solvent the system was introduced into a microprocessor controlled UV irradiation system and irradiated with UV light (365nm) for 1 hour. Subsequently the sample was washed with abundant warm toluene to ensure the elimination of all non-covalently linked species.

The Raman spectra of the CVD graphene monolayer is shown in Figure S11(a), where the typical graphene signals can be perceived, i.e. the first-order G band (1590 cm^{-1}), the second order 2D band (2700 cm^{-1}) and an almost imperceptible disorder-induced D band at 1355 cm^{-1}, respectively.

After the aforementioned treatment some changes can be detected, especially in the relative intensity of the D and G bands (Figure S11 (b)). While in some cases the I_D/I_G ratio is close to that for the untreated sample in many other cases it is significantly higher. These can be interpreted as the result of the creation of sp^3 carbon by covalent attachment of the polymer. Also the changes of the I_D/I_G ratio are accompanied

by the development of a new band at 1627 cm^{-1} that almost overlaps with the G band, denominated the D' band.[10] It is known that in systems with a sufficiently high number of defects, the shape of the band near 1580-1600 cm^{-1} is conditioned by the overlap of the G and D´ mode, the latter associated with phonons that become Raman active due to confinement in the defective structure.[11]

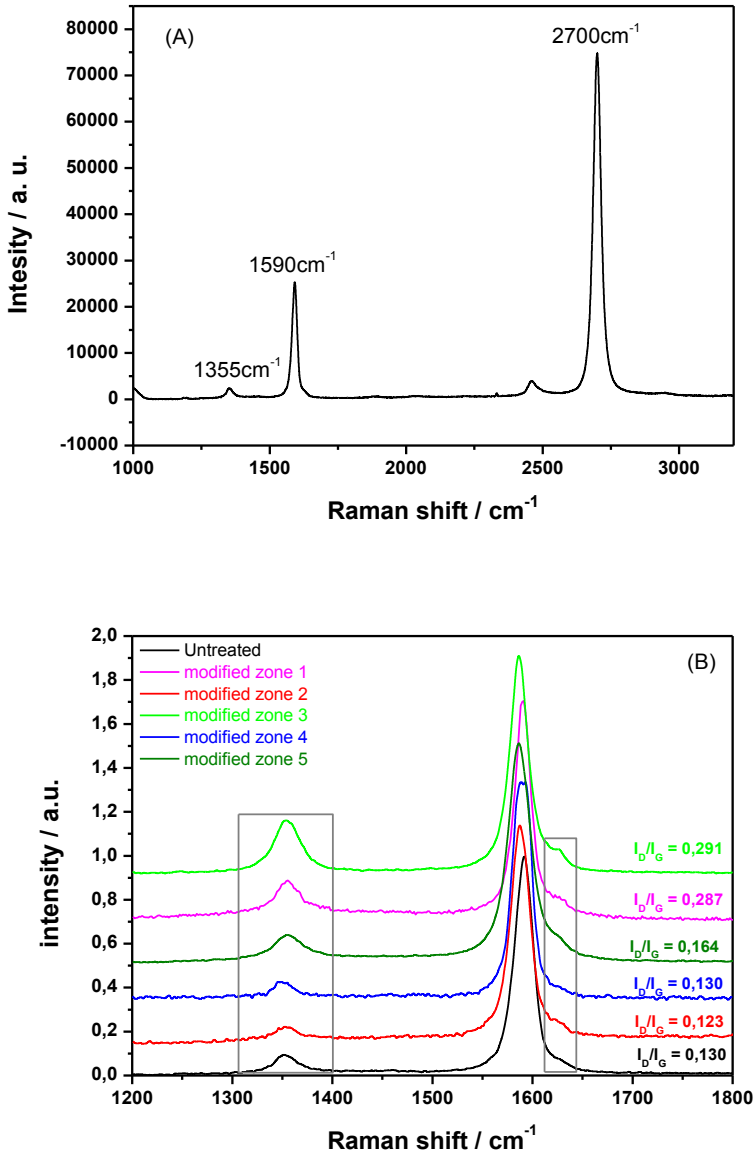

Figure S12. (A) Typical Raman spectrum of CVD grown monolayer graphene on Si/SiO2. (B) Variation of the Raman D and G signals of different regions of the sample in A after photo-initiated thiol-ene reaction. Laser source = 514 nm.

[1] Mazzolini, J. Mokthari, I.; Briquel, R.; Boyron, O.; Delolme, F.; Monteil, V.; Bertin, D.; Gigmes, D.; D'Agosto, F.; Boisson, C. *Macromolecules* **2010**, *43*, 7495

[2] M. Castelaín, G. Martínez, P. Merino, J. A. Martín-Gago, J. L. Segura, G. Ellis, H. J. Salavagione, *Chem. Eur. J.* **2012**, *18*, 4965-4973.
[3] M. Fang,.K. Wang,. H. Lu, Y. Yang, S. Nutt. J. Mater. Chem. **2010**, 20, 1982–1992
[4] H. He, C. Gao, Chem. Mater. **2010**, 22, 5054
[5] J. R. Lomeda , C. D. Doyle , D. V. Kosynkin , W.-F. Hwang, J. M. Tour, J. Am. Chem. Soc. 2008, 130, 16201.
[6] M. Fang,.K. Wang,. H. Lu, Y. Yang, S. Nutt. J. Mater. Chem. 2009, 19, 7098.
[7] S. M. Kang, S. Park, D. Kim, S. Y. Park, R. S. Ruoff, H. Lee, Adv. Funct. Mater. 2011, 21, 108
[8] J. M. Englert, C. Dotzer, G. Yang, M. Schmid, C. Papp, J. M. Gottfried, H.-P. Steinrïck, E. Spiecker, F. Hauke, A. Hirsch, Nat. Chem. 2011, 3, 279.
[9] Marta Castelaín, Peter S. Shuttleworth, Carlos Marco, Gary Ellis, Horacio J. Salavagione, submitted manuscript.
[10] R. Tuinstra, J. L. Koenig, J. Chem. Phys. **1970**, 53, 1126
[11] L. G. Cançado, M. A. Pimenta, B. R. A. Neves, M. S. S. Dantas, A. Jorio, Phys. ReV. Lett. **2004**, 93, 247401